Applied Energy 250 (2019) 404–412

Contents lists available at ScienceDirect

Applied Energy

journal homepage: www.elsevier.com/locate/apenergy

Numerical study on a water cooling system for prismatic $LiFePO_4$ batteries at abused operating conditions

Xinhai Xu[a,*], Wenzheng Li[a], Ben Xu[b], Jiang Qin[c,*]

[a] School of Mechanical Engineering and Automation, Harbin Institute of Technology, Shenzhen 518055, China
[b] College of Engineering and Computer Science, University of Texas Rio Grande Valley, Edinburg, TX 78539, USA
[c] School of Energy Science and Engineering, Harbin Institute of Technology, Harbin 150001, China

HIGHLIGHTS

- A novel modular water cooling system for Li-ion batteries is proposed.
- Cooling performances with different parameters were numerically studied.
- Abused battery operating conditions were considered.
- Battery temperature < 32.5 °C and greatly uniform distribution were obtained.

ARTICLE INFO

Keywords:
Thermal management
Active cooling
Li-ion battery
Cold plate
Temperature distribution

ABSTRACT

Cooling of the Li-ion battery module is a critical issue for electric vehicles in regard with the battery performance and lifetime, particularly at abused operating conditions. A water cooling system consisting of two novel cover plates with T-shape bifurcation structures and eight traditional cold plates was proposed and investigated for cooling of prismatic $LiFePO_4$ battery modules. A computational fluid dynamics simulation model of the cooling system was established and validated by experimental data. The results show that a cold plate with four circular mini-channels flowing water can keep the maximum temperature of a single battery around 35 °C at 1 °C discharging rate and ambient temperature of 40 °C. Effect of the coolant flow rate is much less significant than the inlet coolant temperature on the cooling performance. Two sets of the proposed water cooling systems can significantly reduce the maximum temperature of a battery module consisting of 15 batteries. Moreover, great temperature distribution uniformity between different batteries can be achieved because the novel cover plate is able to distribute water evenly into each mini-channel of the cold plates. The cooling system can keep the maximum temperature of the module below 32.5 °C and the difference between the highest and lowest temperatures around 1.5 °C at abused operating conditions.

1. Introduction

Electric vehicles (EVs) are considered as a promising alternative technology for traditional internal combustion engine vehicles (ICEVs) because of higher energy utilization efficiency and lower emissions of pollutant [1]. The Li-ion battery pack is one of the most important components in EVs as the energy storage unit which can support fast acceleration and long driving mileage. The lifetime, usable capacity and safety of a Li-ion battery pack are significantly influenced by the operating temperature and the temperature difference between individual batteries [2]. In-plane non-uniform temperature distribution in a large single battery can also influence its performance [3]. However, a large amount of heat is generated in EVs during discharging due to chemical reactions and ohmic resistance [4]. Generally, operating temperature in the range of −20 and 60 °C is required for Li-ion batteries to avoid temperature-related degradation and possible thermal runaway [5]. Pesaran et al. [6] suggested a narrower temperature range of 15 and 35 °C to maintain the optimal battery performance. Moreover, the temperature difference between individual cells in a module is required to be less than 5 °C [7]. Therefore, the battery thermal management system (BTMS) is necessary to effectively and efficiently remove excessive heat from the batteries.

Three major cooling techniques for Li-ion batteries are air cooling, liquid cooling and phase change material (PCM) cooling. Besides,

* Corresponding authors.
E-mail addresses: xuxinhai@hit.edu.cn (X. Xu), qinjiang@hit.edu.cn (J. Qin).

https://doi.org/10.1016/j.apenergy.2019.04.180
Received 8 January 2019; Received in revised form 2 April 2019; Accepted 30 April 2019
Available online 09 May 2019

emerging cooling technology such as mist cooling combining forced air and water evaporation [8] and hybrid cooling integrating liquid cooling and PCM [9,10] were also in development. Generally, air cooling and liquid cooling are more commercially mature than PCM cooling. During high discharging rate or high ambient temperature, the passive PCM cooling also has the risk of running out of available latent heat [11]. Although air cooling has advantages including low cost, weight, complexity and ease to maintain, it is not suitable for batteries working at abused operating conditions such as high discharging rate or high ambient temperature due to low heat transfer characteristics of air [12]. Packaging is also an issue of air cooling thermal management systems since a large manifold for air supply is needed [13]. Recent improvements in both air cooling and liquid cooling concentrate in novel design and parametric study of BTMSs to reach optimized heat dissipation performance in regard with low maximum temperature and high temperature uniformity of different batteries in a module.

Numerical simulation is widely employed to investigate the temperature distribution and thermal behavior of Li-ion batteries at various operating conditions [14]. For air cooling of pouch batteries, Park [15] numerically compared the performances of BTMSs with traditional U-shape and Z-shape ducts. Fan et al. [16] numerically studied effects of the gap spacing and air flow rate on thermal management of an air cooling battery module containing eight prismatic Li-ion batteries operating under a modeled aggressive driving profile. It was found that the temperature rise of batteries can be reduced by lowering the gas spacing or increasing the air flow rate. A trade-off is required to achieve the satisfied cooling performance at acceptable fan power consumption. Yu et al. [17] proposed a novel BTMS design with two directional air flows. Numerical and experimental results indicate both the maximum temperature and temperature uniformity are improved. Recently, fins [18] and metal foams [19,20] were embedded into the flow channels in order to enhance heat transfer. Giuliano et al. [21] experimentally studied the performance of an air cooling thermal management system employing metal-foam based heat exchanger plates inserted between adjacent batteries. The temperature rise can be restricted to less than 10 °C for 200 A charging-discharging cycles at the air flow rate of 1100 mL/s. However, it is worth noticing that the tested ambient temperature is only 22 °C. Saw et al. [20] employed the CFD technique to study a metal foam cooling system for Li-ion battery module and optimized pore density and porosity of the metal foam. For liquid cooling, Lan et al. [22] proposed a new BTMS design with mini-channel aluminum tubes twisting around a single Li-ion battery. Water flows inside the mini-channels to cool down the battery. Numerical results show that the maximum temperature of 27.8 °C and temperature difference of only 0.8 °C can be achieved at the discharging rate of 1 C. Zhang et al. [23] further experimentally verified the cooling performance of such a BTMS design for a battery pack. A sheet of flexible graphite was inserted between the cell wall and the tubes in order to enhance heat transfer. Experimental results indicate that great cooling performance was achieved and the temperature difference between batteries was below 5 °C. Another commonly used design concept is to insert a cold plate with mini-channels into neighboring prismatic batteries. Huo et al. [24] and Qian et al. [25] investigated effects of the number of channels, flow direction, and water velocity. Except for straight mini-channels, other types of channels were also investigated. Jarrett and Kim [26] numerically studied and optimized a cold plate with a serpentine channel. Jin et al. [27] examined the cooling performance of a cold plate by adding oblique fins in the straight channels and the results show that heat transfer was greatly enhanced.

Most of the previous research on liquid cooling of prismatic battery modules assumed the coolant entering each cold plate was uniform. However, the method to ensure uniform distribution of coolant in separate cold plates is usually not discussed. Moreover, the maximum temperature and temperature distribution uniformity in a battery module operating at abused conditions, such as high discharging rate and ambient temperature, are not thoroughly investigated. The present study proposed a novel modular designed liquid cooling system consisting of a cover plate to uniformly distribute water in different cold plates. Numerical methods were employed to investigate the cooling performance for a battery module consisting of multiple large capacity (70 Ah) prismatic lithium iron phosphate batteries at 1 °C discharging rate and ambient temperature of 40 °C. Effects of the ambient temperature, number of mini-channel in a cold plate, coolant type, inlet coolant temperature and flow rate were studied.

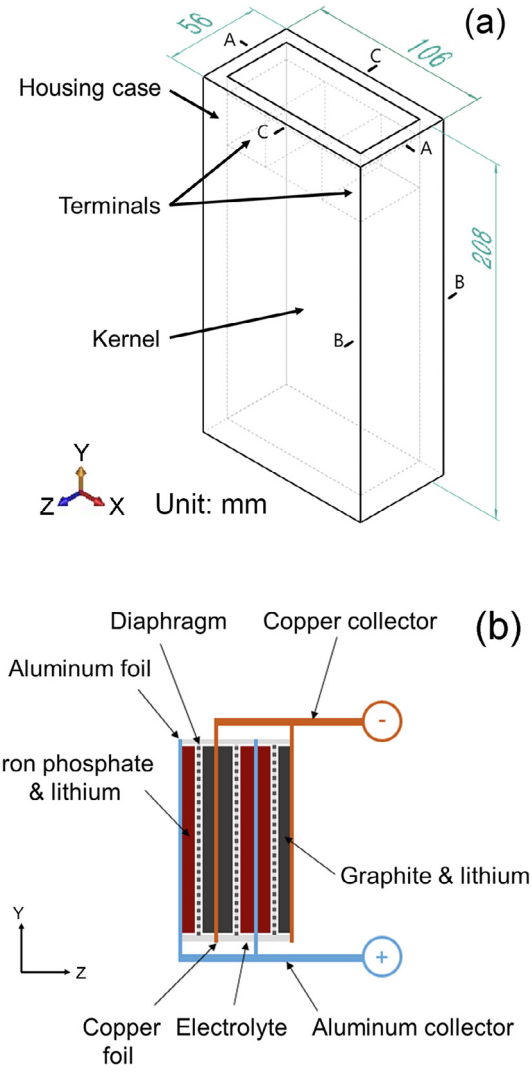

Fig. 1. (a) Dimensions of the simplified battery, and (b) Schematic of the structure and materials of the battery kernel.

2. Methodology

2.1. Battery modeling

The prismatic lithium iron phosphate ($LiFePO_4$) battery was investigated because it is the most commonly used battery type by the largest EV manufacturer of China – BYD Auto [28]. Fig. 1(a) shows dimensions of the simplified battery, which mainly consists of the terminals, kernel and housing case. The studied battery has a capacity of 70 Ah. The structure and materials of the battery kernel is illustrated in Fig. 1(b). The kernel is composed of hundreds of repeating units, which includes the aluminum foil layer, iron phosphate & lithium layer, diaphragm layer, graphite & lithium layer, and copper foil layer. The materials were assumed to be identical in each repeating unit and

Table 1
Parameters of different materials in the studied $LiFePO_4$ battery.

	Iron phosphate	Graphite	Diaphragm with electrolyte	Copper foil	Aluminum foil	Housing case
Thickness, μm	19.9	21.6	3.46	1.3	1.3	8000
Thermal conductivity, W/(m·K)	1.48	1.04	0.38	398	238	0.35
Density, kg/m^3	1200	2500	960	8900	2700	1180
Specific heat, J/(kg·K)	3500	710	2100	390	880	1500

uniform in different directions. Thickness, thermal conductivity, density and specific heat of each layer are listed in Table 1.

Heat generated within the battery during the discharging process includes the heat originated from the battery kernel and the heat produced by the terminals. Bernadi et al. [29] proposed a formula which is widely used to calculate the heat generation in the kernel as shown in Eq. (1).

$$q_k = \frac{I}{V_k}\left(IR_r - T\frac{dU_{OC}}{dT}\right) \quad (1)$$

where q_k is the volumetric heat generation rate of the battery kernel, W/m^3; V_k is the volume of the battery kernel, m^3; I is the discharging current, A; R_r is the internal resistance, Ω; T is the battery temperature, K; and U_{OC} is the open circuit voltage, V. The second term can be neglected in the present study because it contributes to less than 2% of the total heat generation at 1 °C discharging rate.

The heat originated from the terminals is Joule heat which is calculated by [14],

$$q_t = \frac{I^2R_t}{V_t} \quad (2)$$

where q_t is the volumetric heat generation rate of the battery terminal, W/m^3; R_t is the resistance of the terminal, Ω; V_t is the volume of the terminal, m^3. The resistance is 0.1 mΩ and 0.05 mΩ for the positive and negative terminals, respectively.

The overall effective thermal capacity of the battery kernel is calculated based on the equation as follows [29],

$$\rho C_p = \frac{\sum \rho_i C_{p,i} V_i}{\sum V_i} \quad (3)$$

where i denotes each layer of the battery kernel as shown in Fig. 1(b); ρ is the density, kg/m^3; C_p is the specific heat, J/(kg·K); V is the volume, m^3.

The thermal conductivity of the battery kernel is anisotropic because it is stacked by components with different thermal properties. The thermal conductivity of the battery kernel in the x, y directions and z direction as shown in Fig. 1(a) are calculated by Eq. (4) and (5), respectively [30].

$$\lambda_{x,y} = \frac{\sum \lambda_i L_i}{\sum L_i} \quad (4)$$

$$\lambda_z = \frac{\sum L_i}{\sum \frac{L_i}{\lambda_i}} \quad (5)$$

2.2. BTMS design

Fig. 2(a) shows the schematic of the water cooling system for a module consisting of fifteen $LiFePO_4$ batteries, and Fig. 2(b) indicates the explosive view of the cooling system with batteries. The system is composed of two modular sets, and each set has two cover plates and eight parallel cold plates. The cover plates were placed at top and bottom of the battery module for uniform coolant distribution, and each cold plate has four circular mini-channels flowing the coolant. Plexiglass is used for the cover plates in order to reduce weight and aluminum is employed to manufacture the cold plates due to high thermal

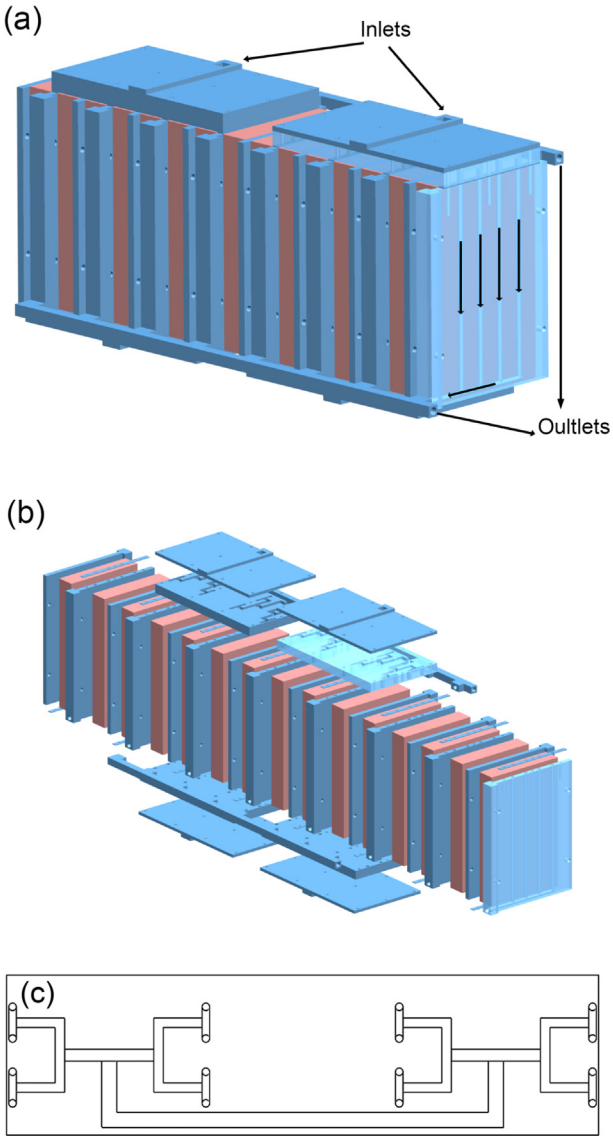

Fig. 2. (a) Schematic of the water cooling system for 15 batteries, (b) explosive view of the cooling system with batteries, and (c) top view of the cover plate with coolant distribution structure.

conductivity. The battery is inserted between two adjacent cold plates, and the coolant in the two cold plates flows in opposite directions. Compression pressure from bolts and nuts is applied to the cold plates and batteries to reduce the contact thermal resistance.

The uniform distribution of cooling water in different cold plates is usually neglected in the literature. The present study proposed the design of T-shape bifurcated structure to evenly distribute water into 16 vertical mini-channels. The design concept was adapted from the authors' previous study on gas uniform distribution [31]. Fig. 2(c) shows the top view of the cover plate with coolant distribution structure. The coolant from one inlet is supposed to be equally divided into the sixteen

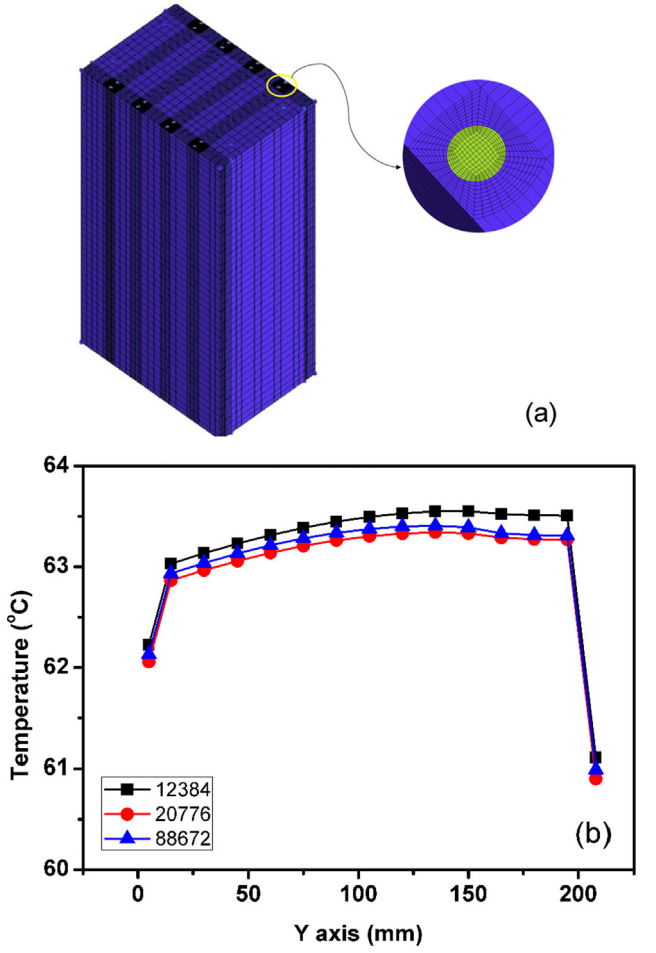

Fig. 3. (a) Grid meshing of a single battery, and (b) Temperature inside the battery along the line of x = 85 mm and z = 28 mm at steady state based on different grid numbers.

mini-channels in the four cold plates. A uniformity index f which characterizes the uniformity of coolant distribution in the sixteen mini-channels is defined by Eq. (6).

$$f = 1 - \left[\frac{1}{16}\sum_{n=1}^{16}\left(\frac{m_i}{m_{ave}} - 1\right)^2\right]^{1/2} \quad (6)$$

where m_i is the coolant mass flow rate in the ith mini-channel, and m_{ave} is the average mass flow rate in the sixteen mini-channels.

2.3. CFD setting

The 3D models were created in Solidworks and then imported into ICEM for meshing. ANSYS Fluent was employed for numerical simulation. UDF was compiled into Fluent to define the heat generation rate. The QUICK scheme was used to solve the convection terms in the convection-diffusion equation. The SIMPLE scheme was employed to solve the pressure-velocity coupling. Natural convection with the heat transfer coefficient of 3.9 W/m^2·K was set for the battery surface exposed to the ambient. The abused ambient temperature was set at 40 °C. The discharging rate of the battery was set at 1 °C.

Fig. 3(a) indicates the grid meshing of the 3D model of a single battery. A hexahedral mesh was employed and the grids were refined in the region close to the circular mini-channel in the cold plate. In order to reduce the computational cost, grid sensitivity study was conducted for a single battery without coolant flowing in the cold plate. Fig. 3(b) shows the temperature inside the battery along the line of x = 85 mm and z = 28 mm at steady state based on the grid numbers of 12,384, 20,776, and 88,872. The relative difference between the temperatures calculated based on the grid numbers of 20,776 and 88,872 is less than 0.2%. Therefore, the grid number for one battery around 20,000 is acceptable for obtaining accurate numerical results.

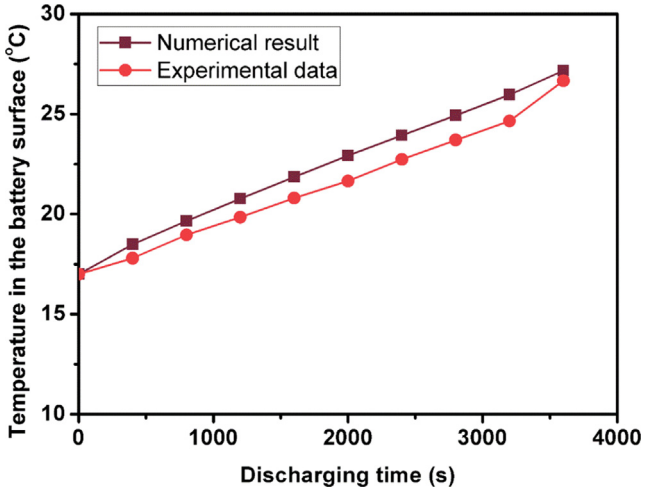

Fig. 4. Numerical validation of the CFD model.

2.4. Validation

The numerical results were validated by comparing the calculated surface temperature with the experimentally measured data for a single $LiFePO_4$ battery without active cooling [32]. The battery was placed in a test chamber with constant temperature of 25 °C. The initial temperature of the battery surface was 17 °C. The battery was discharging at 1 °C by a charge-discharge tester. Fig. 4 shows that the numerical result and experimental data have good agreement and the CFD model was validated.

3. Results and discussion

3.1. Cooling for a single battery

3.1.1. Battery without active cooling

Effect of the ambient temperature on heat generation of a single $LiFePO_4$ battery without active cooling was numerically investigated by varying the ambient temperature from 30 to 45 °C and the discharging rate between 0.4 C and 1 C. Fig. 5 shows that the maximum temperature in the A-A cross section (shown in Fig. 1) of a single battery is significantly influenced by the ambient temperature and the discharging rate. When the ambient temperature is fixed, the maximum battery temperature increases as the discharging rate increases. At 0.4 C discharging rate, passive cooling is able to keep the battery temperature slightly higher than the ambient temperature during discharging. Even at 1 C discharging rate, active heat dissipation is not quite necessary for a single battery if the ambient temperature is 30 °C since the highest temperature of the battery is only 39 °C after 1 h operation. However, the maximum temperature of a single battery can reach 50 °C without active cooling when the ambient temperature is 40 °C at 1 C discharging rate. Moreover, the temperature would further increase if multiple batteries are stacked together as a module.

3.1.2. Active cooling with different numbers of mini-channel and coolants

A traditional cold plate with parallel circular mini-channels was examined for active cooling of the single battery. Thickness of the cold plate is 8 mm and diameter of each circular mini-channel is 5 mm. In order to optimize the number of parallel channels and select the most appropriate coolant material, cooling performance of cold plates with

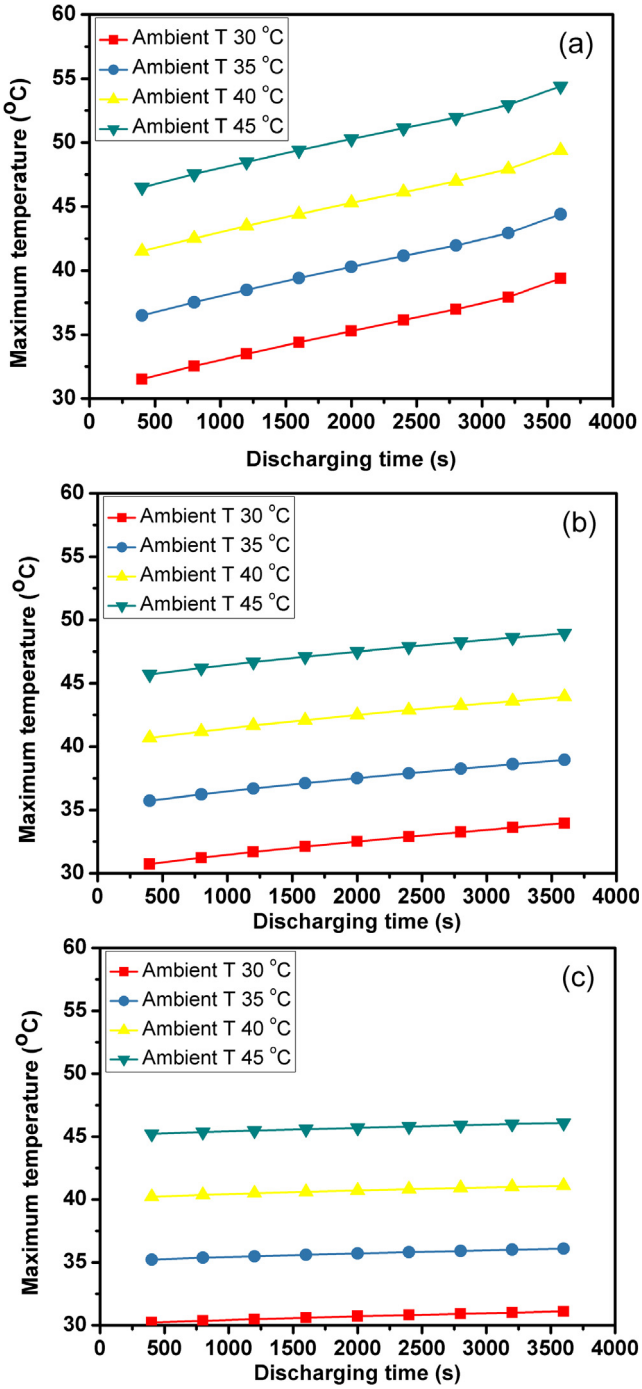

Fig. 5. The maximum battery temperature in the A-A cross section changing with time at different ambient temperatures and the discharging rate of (a) 1 C, (b) 0.7 C, and (c) 0.4 C.

different number of mini-channels and various coolants were numerically evaluated. Fig. 6 compares the maximum temperature in the A-A cross section of a single battery with active cooling. The battery with 1 C discharging rate was sandwiched between two cold plates with identical number of mini-channels. The ambient temperature of 40 °C was considered. Water was used as the coolant and the total mass flow rate for each cold plate was set as 1 g/s regardless of the number of mini-channels. Inlet temperature of the coolant water was 30 °C. The results indicate that the maximum temperature decreases as the number of mini-channels increases from 1 to 4. Fig. 7 compares the effect of various coolants on the cooling performance of the cold plate with four

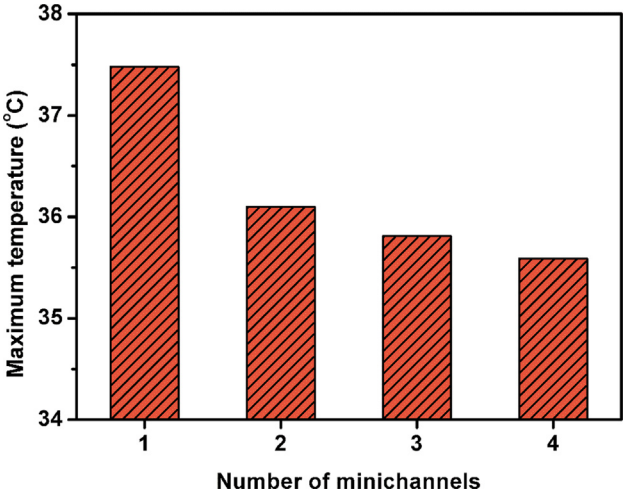

Fig. 6. Effect of the number of channels on the cooling performance.

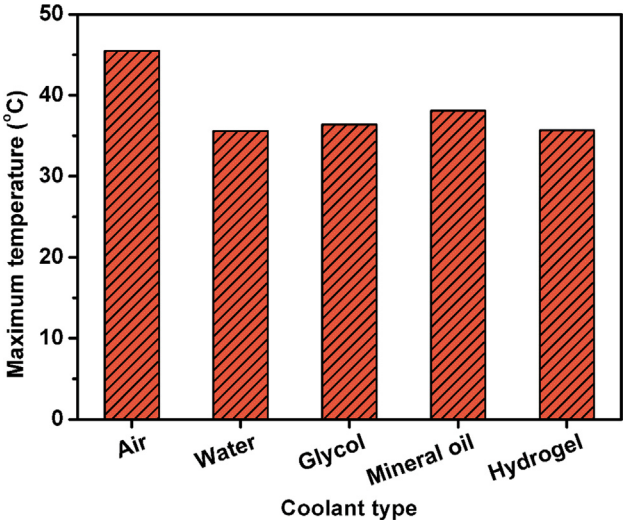

Fig. 7. Effect of the coolant material on the cooling performance.

mini-channels. The inlet temperature and total mass flow rate of each coolant was set as 30 °C and 1 g/s, respectively. It can be seen that the cooling performance of air is the worst due to relatively low convection heat transfer coefficient. The cooling performance of water, glycol, mineral oil and hydrogel is similar, yet the viscosity of mineral oil is high and the cost of hydrogel is expensive compared to water. Both water and glycol can be used as the coolant for active liquid cooling. Moreover, a mixture of water and glycol is preferred in practical applications because glycol can reduce the freezing risk of water at low ambient temperature. Since the ambient temperature considered in the present study is 40 °C, pure water as the coolant was examined in the further studies.

3.2. Cooling for a battery module

3.2.1. Battery module without active cooling

Temperature distribution of a module consisting of fifteen $LiFePO_4$ batteries discharging at 1 °C was examined at 40 °C ambient temperature. Fig. 8(a) shows that the maximum temperature in the battery module can reach 90 °C without active cooling due to severe heat accumulation in the module, which suggests that an active cooling system is absolutely necessary. The batteries in the middle section of the module have the highest temperature because dissipation of heat generated by these batteries is more difficult than the batteries close to the

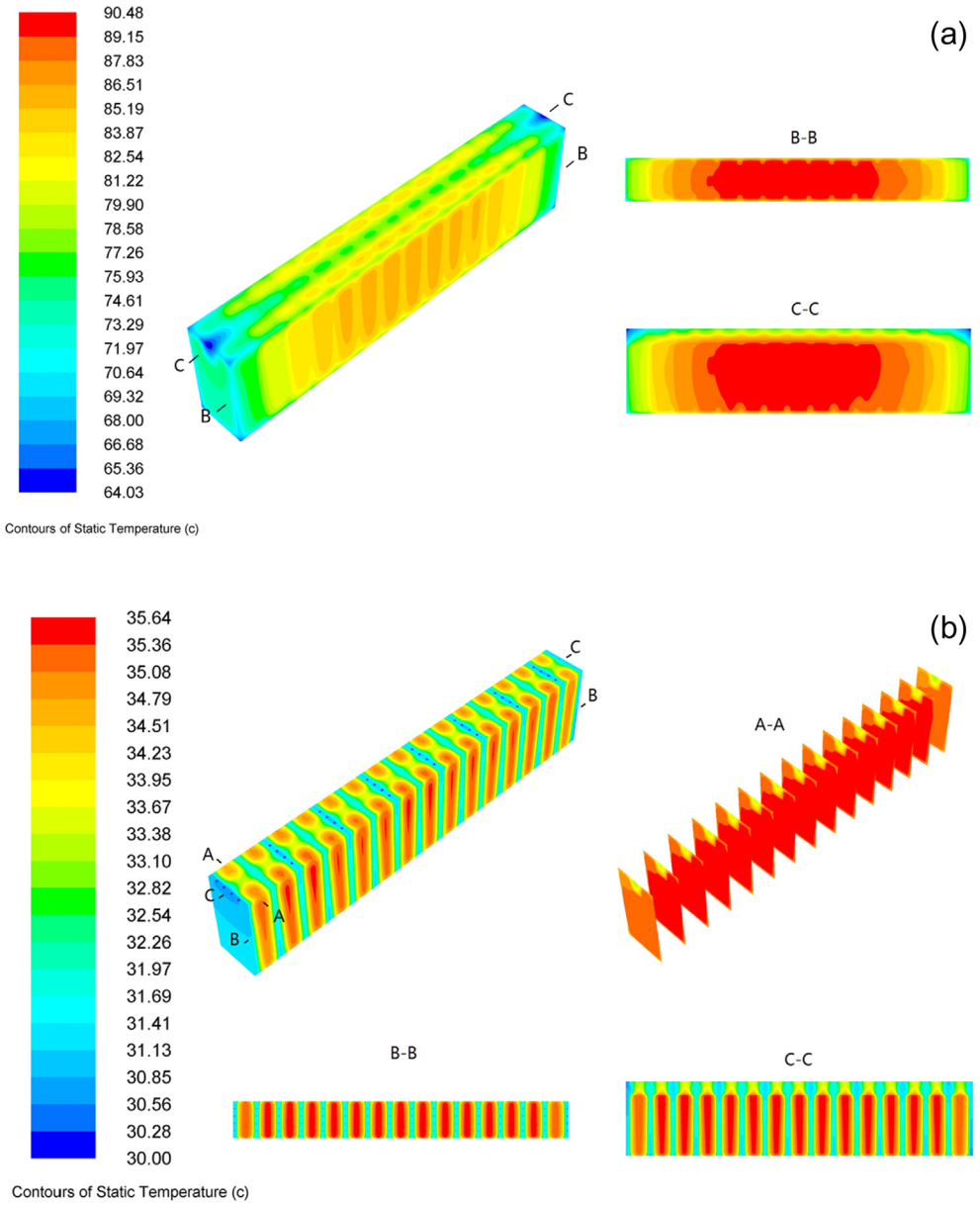

Fig. 8. Temperature distribution in the battery module (a) without active cooling, and (b) with active water cooling system.

edge of the module. Although the batteries at both ends have relatively low temperature, the temperature is still higher than 70 °C. Moreover, the temperature distribution uniformity is far away from the acceptable level. The 20 °C difference between the highest and lowest temperatures in the battery module can significantly worsen the performance and accelerate the degradation of the battery module.

3.2.2. Battery module with active cooling

In order to reduce the maximum temperature and temperature distribution non-uniformity of the battery module, sixteen cold plates were inserted between adjacent batteries. It was assumed that water can enter each mini-channel uniformly. The inlet water temperature was 30 °C, and the mass flow rate is 1 g/s entering each cold plate. Fig. 8(b) shows the temperature distribution in the battery module with such active water cooling system. It can be seen that the maximum temperature of the battery module can be reduced from 90 °C to 35.6 °C, and the difference between the highest and lowest temperatures in the module was reduced from 20 °C to about 1.5 °C. The temperature distribution within each battery is almost identical except for the two batteries at both ends. The batteries at ends of the module have slightly lower temperature than other batteries.

3.2.3. Effect of water inlet temperature

Inlet temperature of the cooling water influences battery temperature of the module. Different inlet water temperatures of 26, 28 and 30 °C were numerical examined and the results are shown in Fig. 9. Fig. 9(a) indicates that average temperature of the A-A cross section of each battery decreases as the inlet water temperature decreases. The average temperature of each battery is below 34 °C when the inlet water temperature is 28 °C, which is in the temperature range for optimal battery performance. The average temperature difference between individual batteries is almost negligible and the temperatures in the end batteries are slightly lower, which is in agreement with Fig. 8(b). Fig. 9(b) shows difference of the highest and lowest temperatures in A-A, B-B, and C-C cross sections of each battery. Temperature difference in the C-C cross section is higher than that in the A-A and B-B cross sections, because the C-C section includes the part between two terminals which has the lowest temperature in the battery. Even so,

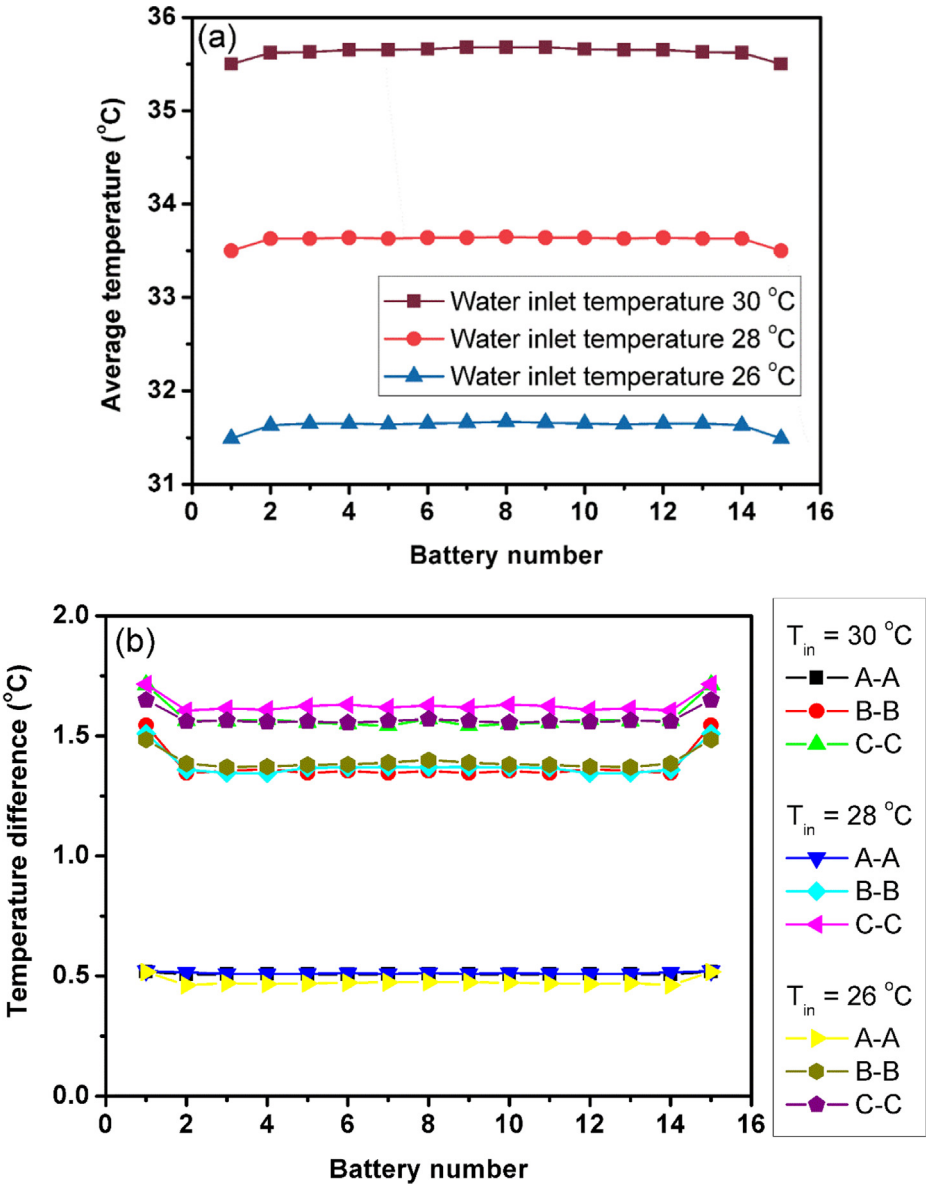

Fig. 9. Effect of the water inlet temperature (a) on the average temperature of the A-A cross section, and (b) on the difference between the highest and lowest temperatures of each battery in the module.

temperature difference in the C-C cross section is still less than 1.8 °C within any battery. The temperature distribution uniformities between different batteries and within single batteries are both greatly improved by the active water cooling system.

3.2.4. Effect of water flow rate

Effect of the water flow rate in each cold plate ranging between 0.2 and 2 g/s on the active cooling performance is shown in Fig. 10. The inlet temperature of water was set as a constant of 30 °C. The result indicates that effect of the water flow rate is less significant than inlet temperature on the cooling performance. As the water flow rate in the cold plate increases from 0.2 to 2 g/s, average temperature in the A-A cross section of each battery only decreases from 36.8 to 35.4 °C.

3.2.5. Performance of the cooling system with cover plates

The aforementioned analyses were conducted based on the assumption that the water flow rate in each mini-channel is identical. However, the uniform distribution of cooling water in different cold plates from one single inlet is a complex engineering problem. The present study proposed a cover plate with novel structure design to

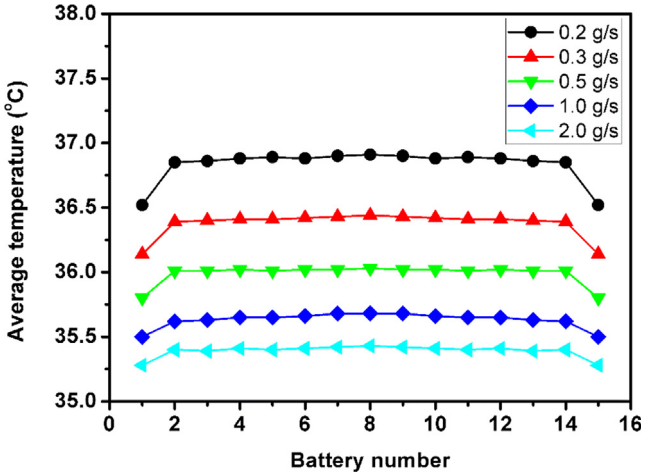

Fig. 10. Effect of the water flow rate on the average temperature of the A-A cross section of each battery in the module.

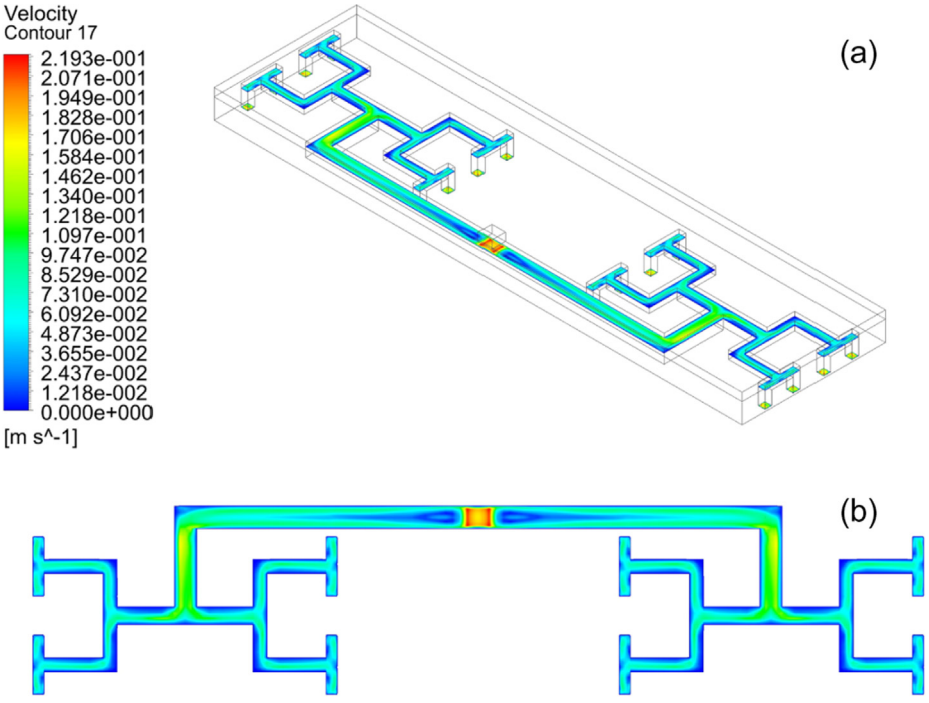

Fig. 11. Velocity contour of water distribution in the cover plate (a) oblique view, and (b) top view.

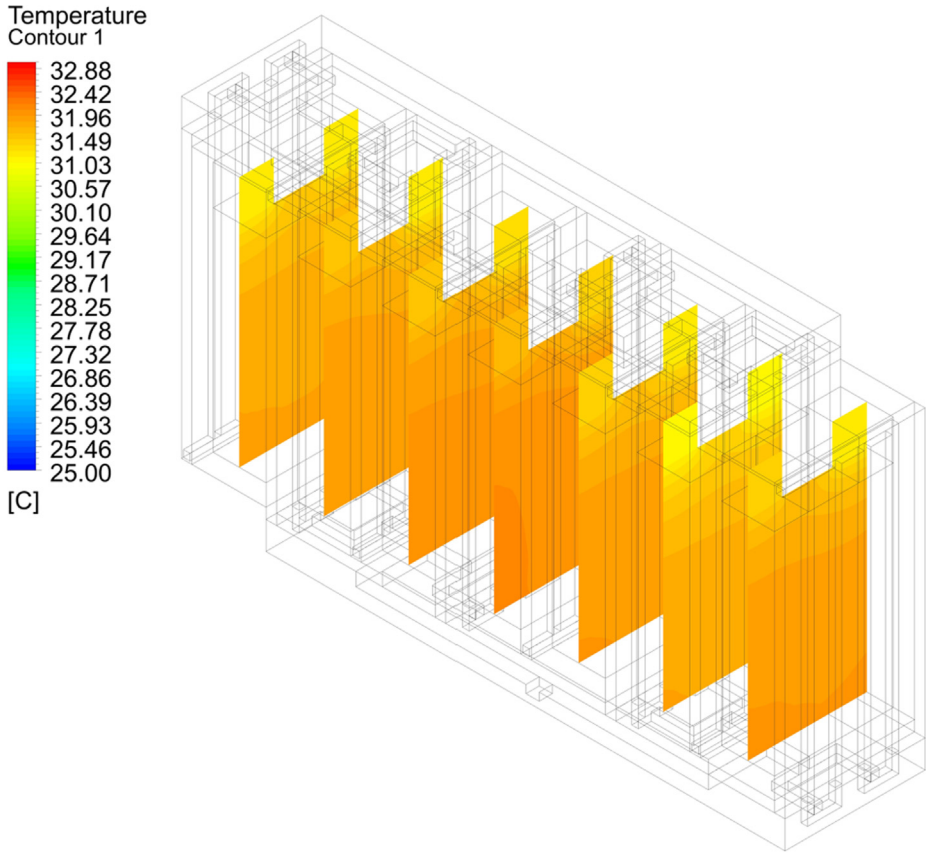

Fig. 12. Temperature distribution in the A-A cross section of each battery in the short module.

distribute water. Fig. 11 shows that the cover plate can distribute water from one inlet into 16 outlets uniformly. The calculated uniformity index is 0.94 (1 means perfect uniformity).

The performance of one set water cooling system with two cover plates and eight cold plates for a short module consisting of seven $LiFePO_4$ batteries was numerically investigated. The discharging rate of each battery, ambient temperature, inlet temperature of the cooling water, and water flow rate in one cold plate are 1 °C, 40 °C, 26 °C and 1 g/s, respectively. Fig. 12 shows the temperature distribution in the A-A cross section of each battery in a short module containing seven

batteries. It can be seen that all the batteries have uniform temperature distribution, which also suggests water is uniformly distributed by the cover plates into each cold plate. The maximum temperature is below 32.5 °C, and the difference between the highest and lowest temperatures is around 1.5 °C.

4. Conclusions

Cooling of the Li-ion battery module is a critical issue for electrical vehicles particularly at abused operating conditions. The present study proposed an active water cooling system and numerically investigated its performance for a prismatic $LiFePO_4$ battery module based on a simplified battery heat generation model. It was found that a traditional cold plate with four mini-channels using water as the coolant can effectively reduce the temperature of a battery module to the optimal temperature range even when the ambient temperature is 40 °C and the discharging rate is 1 °C. The battery temperature can be reduced to 33.5 °C with water inlet temperature of 28 °C and water flow rate of 1 g/s in each cold plate. The difference between the highest and lowest temperature in the module is less than 1.8 °C which corresponds to great temperature distribution uniformity. Effect of the water flow rate is far less significant than the water inlet temperature on the cooling performance. However, multiple cold plates are required and uniform distribution of water from one inlet into the cold plates is a complex engineering problem which is often neglected in previous studies. A novel cover plate with T-shape bifurcation structure was designed in order to achieve uniform water distribution in different cold plates and mini-channels. The performance of one set cooling system consisting of two cover plates and eight cold plates was numerically investigated. The results show that both low maximum temperature and great temperature distribution uniformity can be obtained by the novel cooling system. In the future work, the performance of the cooling system should be experimentally examined, and the influences of the system on the battery performance and life need to be evaluated.

Acknowledgement

Support from National Natural Science Foundation of China (51706056) and Shenzhen Science and Technology Innovation Commission (JCYJ20180306171730206) is gratefully acknowledged.

References

[1] Campanari S, Manzolini G, Iglesia FG. Energy analysis of electric vehicles using batteries or fuel cells through well-to-wheel driving cycle simulations. J Power Sources 2009;186:464–77.
[2] Raijmakers L, Danilov D, Eichel R, Notten P. A review on various temperature-indication methods for Li-ion batteries. Appl Energy 2019;240:918–45.
[3] Klein M, Tong S, Park J. In-plane nonuniform temperature effects on the performance of a large-format lithium-ion pouch cell. Appl Energy 2016;165:639–47.
[4] Liu R, Chen J, Xun J, Jiao K, Du Q. Numerical investigation of thermal behaviors in lithium-ion battery stack discharge. Appl Energy 2014;132:288–97.
[5] Väyrynen A, Salminen J. Lithium ion battery production. J Chem Thermodyn 2012;46:80–5.
[6] Pesaran AA, Santhanagopalan GK. Addressing the impact of temperature extremes on large format Li-ion batteries for vehicle applications. In: 30th international battery seminar. Ft Lauderdale, FL, USA; 2013.
[7] Pesaran AA. Battery thermal models for hybrid vehicle simulations. J Power Sources 2002;110:377–82.
[8] Saw L, Poon H, Thiam H, Cai Z, Chong W, Pambudi N, et al. Novel thermal management system using mist cooling for lithium-ion battery packs. Appl Energy 2018;223:146–58.
[9] Ling Z, Cao J, Zhang W, Zhang Z, Fang X, Gao X. Compact liquid cooling strategy with phase change materials for Li-ion battery optimized using response surface methodology. Appl Energy 2018;228:777–88.
[10] Ling Z, Wang F, Fang X, Gao X, Zhang Z. A hybrid thermal management system for lithium ion batteries combining phase change materials with forced-air cooling. Appl Energy 2015;148:403–9.
[11] Kizilel R, Lateef A, Sabbah R, Farid M, Selman J, Al-Hallaj S. Passive control of temperature excursion and uniformity in high-energy Li-ion battery packs at high current and ambient temperature. J Power Sources 2008;183:370–5.
[12] Liu H, Wei Z, He W, Zhao J. Thermal issues about Li-ion batteries and recent progress in battery thermal management systems: a review. Energy Convers Manage 2017;150:304–30.
[13] Chen KH, Han T, Khalighi B, Klaus P. Air cooling concepts for Li-ion battery pack in cell level. In: Proceedings of the ASME 2017 heat transfer summer conference; 2017. HT2017-4701.
[14] Cicconi P, Landi D, Germani M. Thermal analysis and simulation of a Li-ion battery pack for a lightweight commercial EV. Appl Energy 2017;192:159–77.
[15] Park H. A design of air flow configuration for cooling lithium ion battery in hybrid electric vehicles. J Power Sources 2013;239:30–6.
[16] Fan L, Khodadadi JM, Pesaran AA. A parametric study on thermal management of an air-cooled lithium-ion battery module for plug-in hybrid electric vehicles. J Power Sources 2013;238:301–12.
[17] Yu K, Yang X, Cheng Y, Li C. Thermal analysis and two-directional air flow thermal management for lithium-ion battery pack. J Power Sources 2014;270:193–200.
[18] Mohammadian SK, Zhang Y. Thermal management optimization of an air-cooled Li-ion battery module using pin-fin heat sinks for hybrid electric vehicles. J Power Sources 2015;273:431–9.
[19] Mohammadian SK, Zhang Y. Cumulative effects of using pin fin heat sink and porous metal foam on thermal management of lithium-ion batteries. Appl Therm Eng 2017;118:375–84.
[20] Saw LH, Ye Y, Yew MC, Chong WT, Yew MK, Ng TC. Computational fluid dynamics simulation on open cell aluminum foams for Li-ion battery cooling system. Appl Energy 2017;204:1489–99.
[21] Giuliani MR, Prasad AK, Advani SG. Experimental study of an air-cooled thermal management system for high capacity lithium-titanate batteries. J Power Sources 2012;216:345–52.
[22] Lan C, Xu J, Qiao Y, Ma Y. Thermal management for high power lithium-ion battery by minichannel aluminum tubes. Appl Therm Eng 2016;101:284–92.
[23] Zhang T, Gao Q, Wang G, Gu Y, Wang Y, Bao W, et al. Investigation on the promotion of temperature uniformity for the designed battery pack with liquid flow in cooling process. Appl Therm Eng 2017;116:655–62.
[24] Huo Y, Rao Z, Liu X, Zhao J. Investigation of power battery thermal management by using mini-channel cold plate. Energy Convers Manage 2015;89:387–95.
[25] Qian Z, Li Y, Rao Z. Thermal performance of lithium-ion battery thermal management system by using mini-channel cooling. Energy Convers Manage 2016;126:622–31.
[26] Jarrett A, Kim IY. Design optimization of electric vehicle battery cold plates for thermal performance. J Power Sources 2011;196:10359–68.
[27] Jin LW, Lee PS, Kong XX, Fan Y, Chou SK. Ultra-thin minichannel LCP for EV battery thermal management. Appl Energy 2014;113:1786–94.
[28] The battery that powers BYD cars, buses, and forklift trucks. < http://bydeurope.com/innovations/technology/index.php > .
[29] Bernardi D, Pawlikowski E, Newman J. A general energy balance for battery systems. J Electrochem Soc 1985;132:5–12.
[30] Lin C, Li T, Chen Q. Analysis of the heat dissipation capability influence factors of LiMn2O4-based lithium-ion power battery. Acta Armamentarii 2010;31:88–93. In Chinese.
[31] Dong J, Xu X, Xu B. CFD analysis of a novel modular manifold with multi-stage channels for uniform air distribution in a fuel cell stack. Appl Therm Eng 2017;124:286–93.
[32] Liang J. Research on the heat dissipation of pure EV's battery pack Master Thesis Beijing, China: Tsinghua University; 2011